organics

MDPI

Article

Amphiphilic Fluorescein Triazoles: Synthesis and Visible-Light Catalysis in Water

Alina Artemenko [1], Elza Sultanova [1], Diana Mironova [1], Aliya Akhatova [1], Ekaterina Bondareva [1], Daut Islamov [2], Konstantin Usachev [2], Svetlana Solovieva [3], Vladimir Burilov [1,*] and Igor Antipin [1]

[1] Alexander Butlerov Institute of Chemistry, Kazan Federal University, 18 Kremlevskaya St., 420008 Kazan, Russia; alinkamorning@gmail.com (A.A.); elsultanova123@gmail.com (E.S.); mir_din@mail.ru (D.M.); aliyaakhatova01@gmail.com (A.A.); kb6602926@gmail.com (E.B.); iantipin54@yandex.ru (I.A.)

[2] Laboratory for Structural Studies of Biomacromolecules, FRC Kazan Scientific Center of RAS, 2/31 Lobachevskogo Str., 420111 Kazan, Russia; daut1989@mail.ru (D.I.); k.usachev@kpfu.ru (K.U.)

[3] A.E. Arbuzov Institute of Organic & Physical Chemistry, 8 Arbuzov Str., 420088 Kazan, Russia; evgersol@yandex.ru

* Correspondence: ultrav@bk.ru; Tel.: +7-843-2337344

Abstract: Triazole derivatives of fluorescein-containing *N*,*N*-dimethylaminopropyl fragments and their ammonium salts were synthesized with yields of 74–85%. The resulting compounds exhibit fluorescent properties in the green region of the visible spectrum. The critical aggregation concentration (CAC) was estimated using a pyrene fluorescent probe corresponding to a range of 0.28–1.43 mM, and at concentrations above the CAC, the compounds form stable aggregates ranging from 165 to 202 nm. A relative quantum yield of 5–24% has been calculated based on fluorescence and UV spectra. The best value is shown by a derivative containing a tetradecyl substituent. When studying the photocatalytic properties of synthesized compounds through the reaction between *N*-substituted 1,2,3,4-tetrahydroisoquinoline and malonic ester, the mono-tetradecyl derivative demonstrated the best results. According to gas chromatography–mass spectrometry (GC-MS) data, the conversion of the initial heterocycle reached 95%. Therefore, these resulting compounds have the potential to act as an effective photocatalysts.

Keywords: CuAAC; photocatalysis; fluorescein derivatives; aggregation

check for updates

Citation: Artemenko, A.; Sultanova, E.; Mironova, D.; Akhatova, A.; Bondareva, E.; Islamov, D.; Usachev, K.; Solovieva, S.; Burilov, V.; Antipin, I. Amphiphilic Fluorescein Triazoles: Synthesis and Visible-Light Catalysis in Water. *Organics* **2024**, *5*, 346–360. https://doi.org/10.3390/org5030018

Academic Editor: Kirpal Bisht

Received: 18 July 2024
Revised: 5 August 2024
Accepted: 30 August 2024
Published: 11 September 2024

Copyright: © 2024 by the authors. Licensee MDPI, Basel, Switzerland. This article is an open access article distributed under the terms and conditions of the Creative Commons Attribution (CC BY) license (https://creativecommons.org/licenses/by/4.0/).

1. Introduction

"Green (sustainable) chemistry" is attractive to modern organic synthesis due to a range of benefits relative to classical organic synthesis, including milder reaction conditions, an absence of toxic solvents or catalysts, and a short reaction time [1,2]. Therefore, growing attention is being paid to the development of environmentally friendly catalysts, the use of aqueous solutions as a medium, the use of microwave, sono- and, in particular, photocatalysis. Since light, including sunlight, is the source of energy in photocatalytic processes, fluorophores—molecules with fluorescent properties—play an important role [3]. The selection of an appropriate photocatalytic system remains a significant challenge. The variety of reactions that can be accelerated by photocatalysts is extensive, and most research focuses on the photocatalytic treatment of wastewater [4–9]. However, there are publications dedicated to the synthesis of various compounds. For example, benzothiophens [10] and carboxylic acids [11], as well as C-C [12,13] or C-N [14,15] cross-coupling reactions, were successfully synthesized using photoredox catalysis.

Xanthene dyes, such as fluorescein, are widely used as chemosensors [16–18], photocatalysts [19–21], and photosensitizers [22,23] due to their high quantum yield [24]. Additionally, fluorescein can undergo modification through various substitutions of the phenolic and carboxylic groups, resulting in a diverse range of derivatives [25]. Combining

photoredox catalysis with the reaction in aqueous media will bring us even closer to the concept of Green chemistry and is a very important trend [26]. Among the reactions carried out in water, reactions on water (when water does not solvate the reactants) and in water are distinguished [27]. In the latter case, the reaction can be significantly accelerated by the addition of solubilizing amphiphilic additives. Therefore, the synthesis of amphiphilic compounds from fluorescein derivatives allows for the formation of highly organized structures. These structures, on the one hand, have the ability to solubilize organic molecules in water, and, on the other hand, are capable of entering into an excited state upon exposure to quanta of light. This ability enables them to catalyze organic reactions. Thus, it is feasible to integrate micellar and photocatalytic processes within a single catalytic system, thereby enhancing reaction efficiency [28]. However, examples of such systems are still rare [29].

Here, we report on the synthesis of new 1,2,3-triazoles combining fluorescein fragments and dimethylaminopropyl groups using the CuAAC (copper-assisted alkyne-azide cycloaddition) reaction, as well as the production of their ammonium salts. Photophysical properties (quantum yield, fluorescence, and UV absorption spectra) and self-assembly (CAC) properties were studied. Based on the collected data, the photocatalytic activity of the synthesized compounds was studied in model condensation reactions between *N*-phenyl-1,2,3,4-tetrahydroisoquinoline and malonic ester.

2. Materials and Methods

2.1. Synthesis

All reagents were purchased from either Acros, Sigma-Aldrich, or Maclin and used without further purification. The solvents were purified by standard methods. Substance purity and the reaction process were monitored by TLC on Merck UV 254 plates and visualized by exposure to UV with a VL-6.LC lamp (Vilber, Paris, France).

Flash chromatography was conducted using a SepaBean^{TM} machine 2 (Santai Technologies Inc., Montréal, QC, Canada); detector: DAD variable UV (254 and 280 nm); flow range 5 mL/min; gradient $H_2O \rightarrow$ AcN; column type: SepaFlash^{TM} SW004 Bonded, spherical C18, 20–45 µm, 100 Å, item number: SW-5222-004-SP (Santai Technologies Inc., Montréal, QC, Canada).

Melting points were measured using the OIptimelt MPA100 melting-point apparatus (Stanford Research Systems, Sunnyvale, CA, USA).

^{1}H and ^{13}C NMR spectra were recorded on a Bruker Avance 400 Nanobay (Bruker Corporation, Billerica, MA, USA) with signals from residual protons of DMSO-d6 or $CDCl_3$ as the internal standard.

ATR-IR spectra and IR spectra in KBr pellets were collected using a Bruker Vector-22 spectrometer (Bruker Corporation, Billerica, MA, USA).

High-resolution mass spectra with electrospray ionization (HRESI MS) were obtained on an Agilent iFunnel 6550 Q-TOF LC/MS (Agilent Technologies, Santa Clara, CA, USA). The carrier gas was nitrogen, with a temperature of 300 °C, a carrier flow rate of 12.l $\times$ min^{-1}, a nebulizer pressure of 275 kPa, a funnel voltage of 3500 V, a capillary voltage 500 V, a total ion current recording mode, a 100–3000 m/z mass range, and a scanning speed 7 spectra $\times$ s^{-1}.

The data set for single crystal **5** was collected on a Rigaku XtaLab Synergy S instrument with a HyPix detector and a PhotonJet microfocus X-ray tube using Cu Kα (1.54184 Å) radiation at room temperature. Images were indexed and integrated using the CrysAlisPro data-reduction package. Data were corrected for systematic errors and absorption using the ABSPACK module, with numerical absorption correction based on Gaussian integration over a multifaceted crystal model and empirical absorption correction based on spherical harmonics according to the point group symmetry using equivalent reflections. The GRAL module was used for the analysis of systematic absences and space group determination. The structure was solved by direct methods using SHELXT [30] and refined by the full-matrix least squares on F^2 using SHELXL [31]. Non-hydrogen atoms were refined anisotropically. The hydrogen atoms were inserted at the calculated positions and refined

as riding atoms. The figures were generated using the Mercury 4.1 [32] program. Crystals were obtained by the slow evaporation method.

Prop-2-yn-1-yl 2-(3-oxo-6-(prop-2-yn-1-yloxy)-3*H*-xanthen-9-yl)benzoate 2 [33], methyl 2-(6-methoxy-3-oxo-3*H*-xanthen-9-yl)benzoate 3 [34], 3′-hydroxy-6′-methoxy-3*H*-*spiro*[isobenzofuran-1,9′-xanthen]-3-one 4 [35], and 3-azido-*N*,*N*-dimethylpropan-1-amine 7 [36] were synthesized according to the literature procedures.

2.1.1. The Synthesis of Prop-2-yn-1-yl 2-(6-methoxy-3-oxo-3H-xanthen-9-yl)benzoate **5**

To a solution of 3′-hydroxy-6′-methoxy-3H-*spiro*[isobenzofuran-1,9′-xanthen]-3-one **4** (1.5 g, 4.3 mmol, 1 eq.) in 20 mL of dry DMF was added K_2CO_3 (0.89 g, 6.45 mmol, 1.5 eq.). The mixture was stirred at rt for 30 min, and then, propargyl bromide (0.62 g, 5.2 mol, 1.2 eq.) was added. The mixture was stirred for 24 h at rt, and the resultant product was concentrated under vacuum. The residue was suspended in H_2O and the formed precipitate was filtered off. After recrystallization in benzene, product **5** was obtained as orange crystals. The yield was 1.42 g, 85%. Mp = 214 °C.

For ^{1}H NMR (400 MHz, $CDCl_3$, 25 °C) δ, the ppm was 2.33 (t, *J* = 6.9 Hz, 1H, -C≡CH), 3.92 (s, 3H, -OCH_3), 4.59 (dABq, 2H, $\Delta\delta_{AB}$ = 0.07, J_{AB} = 12.2 Hz, *J* = 2.4 Hz, 2H, -OCH_2-), 6.45 (s, 1H, ArH), 6.54 (d, *J* = 9.7, 1H, ArH), 6.74 (d, *J* = 9.0 Hz, 1H, ArH), 6.80–6.92 (m, 2H, ArH), 6.96 (d, *J* = 2.4 Hz, 1H, ArH), 7.34 (d, *J* = 7.2 Hz, 1H, ArH), 7.76 (t, *J* = 7.4 Hz, 1H, ArH), 7.69 (t, *J* = 7.6 Hz, 1H, ArH), 8.27 (d, *J* = 7.8 Hz, 1H, ArH). For ^{13}C NMR (101 MHz, $CDCl_3$, 25 °C) δ, the ppm was 52.9, 56.1, 56.5, 75.5, 100.5, 105.9, 113.6, 113.6, 114.9, 117.9, 128.9, 129.8, 130.2, 130.3, 130.8, 131.5, 133.2, 134.9, 149.7, 154.5, 159.1, 164.2, 164.6, 185.9. IR (KBr) ν_{max} cm^{-1}: 3294 (C≡CH), 2123, 1726 (C=O), 1643, 1599, 1545, 1518, 1481, 1464, 1417, 1379, 1344, 1280, 1269, 1253, 1211, 1130, 1107, 758. For HRESI MS (*m*/*z*) $[M + H]^+$, calcd. for $C_{24}H_{17}O_5^+$ 385.1076, 385.1080 was found (Figure S1 in the Supplementary Materials).

For the crystal data for $C_{24}H_{16}O_5$ (*M* = 384.37 g/mol), monoclinic, space group $P2_1/c$ (no. 14), *a* = 14.5495(3) Å, *b* = 8.7385(2) Å, *c* = 14.4494(3) Å, *β* = 99.790(2)°, *V* = 1810.36(7) $Å^3$, *Z* = 4, *T* = 100.0(7) K, μ(Cu Kα) = 0.815 mm^{-1}, *Dcalc* = 1.410 g/cm^3, 12169 reflections measured (6.164° ≤ 2Θ ≤ 151.978°), 3662 unique (R_{int} = 0.0265, R_{sigma} = 0.0241) were used in all calculations. The final R_1 was 0.0395 (I > 2σ(I)), and wR_2 was 0.1039 (all data). The CCDC number is 2358771.

2.1.2. General Procedure for Synthesis of 1,2,3-triazoles **8**–**9**

To a solution of azide **7** (1 mmol, 1 eq. in case of **5** or 2 mmol, 2 eq. in case of **2**) in 5 mL of THF was added NEt_3 (0.5 mL), followed by alkynes **2** or **5** (1 mmol, 1 eq.) and CuI (0.1 mmol, 0.1 eq.). The reaction mixture was stirred at rt in an inert atmosphere for 10–14 h. The completion of the reaction was determined by TLC ($CHCl_3$:MeOH = 10:1). The reaction mixture was evaporated, diluted with $CHCl_3$, and filtered through amberlite IRA-67®. After evaporation in vacuo, the product was obtained as vitreous oil.

2.1.3. (1-(3-(Dimethylamino)propyl)-1H-1,2,3-triazol-4-yl)methyl 2-(6-((1-(3-(dimethylamino)propyl)-1H-1,2,3-triazol-4-yl)methoxy)-3-oxo-3H-xanthen-9-yl)benzoate **8**

The yield was 0.33 g, 66%. ^{1}H NMR (400 MHz, $CDCl_3$, 25 °C) δ, ppm: 1.98 (*p*, *J* = 6.9 Hz, 2H, -CH_2-), 2.07 (*p*, *J* = 6.9 Hz, 2H, -CH_2-), 2.18 (s, 6H, 2*N-CH_3), 2.20 (s, 6H, 2*N-CH_3), 2.23–2.29, (m, 4H, 2* -NCH_2-), 4.27–4.42 (m, 2H, -NCH_2-), 4.28–4.40 (m, 2H, -NCH_2-), 5.11 (ABq, 2H, $\Delta\delta_{AB}$ = 0.07, J_{AB} = 12.6 Hz, 2H, -OCH_2-), 5.32 (s, 2H, -OCH_2-), 6.39 (s, 1H, ArH), 6.49 (d, *J* = 9.7 Hz, 1H, ArH), 6.76–6.81 (m, 2H, ArH), 6.81–6.89 (m, 1H, ArH), 7.05 (s, 1H, ArH), 7.25 (s, 1H, TrzH), 7.62–7.77 (m, 3H, ArH + TrzH), 8.25 (d, *J* = 7.8, 1.5 Hz, 1H, ArH). ^{13}C NMR (101 MHz, $CDCl_3$, 25 °C) δ, ppm: 28.1, 28.2, 45.4, 45.4, 48.2, 48.4, 55.8, 55.8, 58.5, 62.7, 76.8, 77.2, 77.5, 101.6, 105.7, 113.8, 117.8, 123.7, 123.9, 129.1, 129.9, 129.9, 130.2, 130.3, 130.6, 131.5, 132.9, 134.4, 142.6, 158.9, 162.7, 165.3, 185.6. IR (KBr) ν_{max} cm^{-1}: 3422, 1718 (C=O), 1641, 1597, 1506, 1381, 1344, 1280, 1253, 1209, 1109, 1003, 852, 760. HRESI MS (*m*/*z*) $[M + H]^+$: calcd. for $C_{36}H_{41}N_8O_5^+$: 665.3200, found: 665.3200 (Figure S2 in the Supplementary Materials).

2.1.4. (1-(3-(Dimethylamino)propyl)-1H-1,2,3-triazol-4-yl)methyl 2-(6-methoxy-3-oxo-3H-xanthen-9-yl)benzoate **9**

The yield was 0.4 g, 78%. ^{1}H NMR (400 MHz, $CDCl_3$, 25 °C) δ, ppm: 1.98 (t, *J* = 6.9 Hz, 2H, -CH_2-), 2.19 (m, 8H, 2* NCH_3, -CH_2-), 3.93 (s, 3H, -OCH_3), 4.29–4.38 (m, 2H, -NCH_2-), 5.14 (ABq, 2H, $\Delta\delta_{AB}$ = 0.07, J_{AB} = 12.5 Hz, 2H, -OCH_2-), 6.40 (s, 1H, ArH), 6.49 (d, *J* = 9.8 Hz, 1H, ArH), 6.72 (dd, *J* = 8.9, 2.5 Hz, 1H, ArH), 6.80–6.89 (m, 2H, ArH), 6.84 (dd, *J* = 18.7, 9.3 Hz, 1H, ArH), 7.30 (d, *J* = 5.3 Hz, 2H, ArH + TrzH), 7.67 (t, *J* = 7.1 Hz, 1H, ArH), 7.74 (t, *J* = 6.8 Hz, 1H, ArH), 8.25 (d, *J* = 6.8 Hz, 1H, ArH). ^{13}C NMR (101 MHz, $CDCl_3$, 25 °C) δ, ppm: 28.1, 45.4, 48.1, 55.8, 56.1, 58.5, 100.4, 105.6, 113.5, 114.8, 117.5, 123.9, 128.9, 129.8, 130.2, 130.3, 130.5, 131.4, 132.9, 134.4, 141.4, 150.1, 154.3, 158.9, 164.2, 165.3, 185.5. IR (KBr) ν_{max} cm^{-1}: 3422, 2947, 1720 (C=O), 1643, 1599, 1514, 1464, 1381, 1346, 1280, 1267, 1255, 1211, 1107, 1076, 1026, 852, 758. HRESI MS (*m*/*z*) $[M + H]^+$: calcd. for $C_{29}H_{29}N_4O_5^+$: 513.2138, found: 513.2139 (Figure S3 in the Supplementary Materials).

2.1.5. General Procedure for the Synthesis of Ammonium Salts **10ab**, **11ab**

To a solution of 1,2,3-triazole (0.3 mmol) in 5 mL of fresh distilled MeCN was added alkylbromide (2 eq. in cases of **8** or 1 eq. in case of **9**). The reaction mixture was stirred under reflux for 15–30 h, and the completion of the reaction was determined by HRESI MS. After evaporation of the solvent, the product was concentrated under reduced pressure. The residue was purified by flash chromatography (H_2O:MeOH 100:0–0:100) to afford the pure product.

2.1.6. *N*-(3-(4-(((2-(6-((1-(3-(butyldimethylammonio)propyl)-1H-1,2,3-triazol-4-yl) methoxy)-3-oxo-3H-xanthen-9-yl)benzoyl)oxy)methyl)-1H-1,2,3-triazol-1-yl)propyl)-*N*,*N*-dimethylbutan-1-aminium Bromide **10a**

It was synthesized for 20 h, a yield of 0.239 g, 85%.^{1}H NMR (400 MHz, $CDCl_3$, 25 °C) δ, ppm: 0.81–0.93 (m, 6H, 2*CH_3), 1.10–1.17 (m, 2H, CH_2), 1.26–1.36 (m, 4H, 2*-CH_2), 1.52–1.63 (m, 2H, 2*-CH_2), 1.88 (s, 10H, -CH_2-), 2.33–2.37 (m, 2H, -CH_2-), 2.42–2.51 (m, 2H, -CH_2-), 3.08 (s, 6H, 2*N-CH_3), 3.13 (s, 6H, 2*N-CH_3), 3.18–3.23 (m, 2H, -CH_2-), 3.59 (t, *J* = 5.1 Hz, 2H, -CH_2-), 4.27–4.45 (m, 2H, -CH_2Trz-), 4.49–4.55 (m, 2H, -CH_2Trz-), 4.96 (ABq, 2H, $\Delta\delta_{AB}$ = 0.07, J_{AB} = 12.5 Hz, 2H, -OCH_2-), 5.25 (s, 2H, -OCH_2-), 6.23 (s, 1H, ArH), 6.33 (d, *J* = 9.7 Hz, 1H, ArH), 6.66 (d, *J* = 8.5 Hz, 1H, ArH), 6.71–6.79 (m, 2H, ArH), 7.03 (d, *J* = 2.4 Hz, 1H, ArH), 7.21 (d, *J* = 7.2 Hz, 2H, ArH), 7.35 (s, 1H, TrzH), 7.61 (t, *J* = 7.1 Hz, 1H, ArH), 7.65 (t, *J* = 7.8 Hz, 1H, ArH), 8.15 (d, *J* = 9.4 Hz, 1H, ArH), 8.38 (s, 1H, TrzH). ^{13}C NMR (101 MHz, $CDCl_3$, 25 °C) δ, ppm: 1.4, 1.6, 1.8, 1.9, 2.2, 2.4, 13.9, 14.5, 19.9, 23.0, 24.8, 29.7, 30.0, 32.2, 51.4, 58.4, 62.0, 65.0, 101.6, 105.5, 114.6, 115.3, 116.9, 117.8, 125.1, 129.4, 130.3, 130.7, 130.9, 131.7, 133.3, 134.1, 141.6, 142.8, 151.2, 154.5, 159.4, 163.2, 165.6, 185.7. IR (KBr) ν_{max} cm^{-1}: 3414, 2961, 2928, 1720 (C=O), 1641, 1597, 1502, 1464, 1380, 1346, 1282, 1253, 1211, 1111, 1043, 945. HRESI MS (*m*/*z*) $[M]^{2+}$: calcd. for $C_{44}H_{58}N_8O_5^{2+}$: 389.2260, found: 389.2261 (Figure S4 in the Supplementary Materials).

2.1.7. *N*-(3-(4-(((2-(6-((1-(3-(dimethyl(tetradecyl)ammonio)propyl)-1H-1,2,3-triazol-4-yl)methoxy)-3-oxo-3H-xanthen-9-yl)benzoyl)oxy)methyl)-1H-1,2,3-triazol-1-yl) propyl)-*N*,*N*-dimethyltetradecan-1-aminium Bromide **10b**

It was synthesized for 30 h, with a yield of 0.270 g, 74%. ^{1}H NMR (400 MHz, $CDCl_3$, 25 °C) δ, ppm: 0.85 (t, *J* = 6.7 Hz, 6H, 2*CH_3), 1.21 (s, 48H, -CH_2-), 1.71 (s, 4H, -CH_2-), 2.50–2.53 (m, 2H, -CH_2-), 2. 58–2.69 (m, 2H), 3.30 (s, 6H, 2*N-CH_3), 3.35 (s, 6H, 2*N-CH_3), 3.39–3.49 (m, 4H, 2*-CH_2-), 3.83–3.92 (m, 4H, 2*-CH_2-), 4.49–4.62 (m, 2H, -CH_2Trz-), 4.72 (t, *J* = 6.9 Hz, 2H, -CH_2Trz-), 4.98 (ABq, 2H, $\Delta\delta_{AB}$ = 0.1, J_{AB} = 12.5 Hz, 2H, -OCH_2-), 5.32–5.35 (m, 2H, -OCH_2-), 6.36 (s, 1H, ArH), 6.46 (d, *J* = 9.9 Hz, 1H, ArH), 6.76 (d, *J* = 9.0 Hz, 1H, ArH), 6.79–6.86 (m, 2H, ArH), 7.14–7.19 (m, 1H, ArH), 7.25 (s, 1H, TrzH), 7.49 (d, 1H, ArH), 7.63–7.76 (m, 2H, ArH), 8.23 (d, *J* = 7.8 Hz, 1H, ArH), 8.59 (s, 1H, TrzH). ^{13}C NMR (101 MHz, $CDCl_3$, 25 °C) δ, ppm: 14.2, 22.8, 22.9, 24.0, 24.1, 26.4, 26.6, 28.8, 29.3, 29.5, 29.6, 29.7, 29.8, 29.9, 32.0, 46.9, 47.2, 50.9, 51.3, 58.2, 61.7, 61.8, 62.5, 65.4, 101.5, 105.1, 114.8, 115.1, 117.5, 124.7, 125.8, 129.3, 130.1, 130.2, 130.3, 130.8, 131.6, 133.7, 141.2, 142.5, 151.6, 154.3, 158.9,

163.2, 165.3, 184.7. IR (KBr) ν_{max} cm^{-1}: 3418, 2924, 2880, 2853, 1720 (C=O), 1643, 1597, 1506, 1468, 1381, 1280, 1253, 1211, 1109, 758. HRESI MS (*m*/*z*) $[M]^{2+}$: calcd. for $C_{64}H_{98}N_8O_5^{2+}$: 529.3825, found: 529.3882 (Figure S5 in the Supplementary Materials).

2.1.8. *N*-(3-(4-(((2-(6-methoxy-3-oxo-3H-xanthen-9-yl)benzoyl)oxy)methyl)-1H-1,2,3-triazol-1-yl)propyl)-*N*,*N*-dimethylbutan-1-aminium Bromide **11a**

It was synthesized for 15 h, with a yield of 0.16 g, 79%. ^{1}H NMR (400 MHz, DMSO-d_6, 25 °C) δ, ppm: 0.92 (t, *J* = 7.3 Hz, 3H, CH_3), 1.28 (h, *J* = 7.4 Hz, -CH_2-), 1.59 (*p*, *J* = 8.3 Hz, 2H, -CH_2-), 2.17–2.29 (m, 2H, -NCH_2-), 3.01 (s, 6H), 3.21–3.29 (m, 4H, -CH_2-), 3.92 (s, 3H, -OCH_3), 4.36 (t, *J* = 7.1 Hz, 2H, -NCH_2-), 5.07 (ABq, 2H, $\Delta\delta_{AB}$ = 0.09, J_{AB} = 12.5 Hz, 2H, -OCH_2-), 6.19 (d, *J* = 1.9 Hz, 1H, ArH), 6.34 (d, *J* = 9.7Hz, 1H, ArH), 6.74 (d, *J* = 9.7 Hz, 1H, ArH), 6.82 (d, *J* = 8.9 Hz, 1H, ArH), 6.79–6.86 (m, 2H, ArH), 7.18 (d, *J* = 2.5 Hz, 1H, ArH), 7.49 (d, *J* = 7.5 Hz, 1H, ArH), 7.49 (t, *J* = 7.7 Hz, 1H, ArH), 7.87 (t, *J* = 7.7 Hz, 1H, ArH), 7.92 (s, 1H, TrzH), 8.18 (d, *J* = 9.3 Hz, 1H, ArH). ^{13}C NMR (101 MHz, DMSO-d_6, 25 °C) δ, ppm: 13.5, 19.1, 22.9, 23.6, 46.4, 50.2, 56.3, 57.9, 60.0, 62.9, 100.5, 104.5, 113.4, 114.3, 116.7, 124.8, 128.9, 129.3, 129.5, 130.1, 130.7, 133.3, 133.6, 140.8, 149.6, 153.6, 158.3, 163.9, 164.7, 183.8. IR (KBr) ν_{max} cm^{-1}: 3418, 2961, 1720 (C=O), 1643, 1599, 1508, 1479, 1383, 1346, 1282, 1255, 1215, 1109, 854, 760. HRESI MS (*m*/*z*) $[M]^+$: calcd. for for $C_{33}H_{37}N_4O_5^+$: 569.2758, found: 569.2754 (Figure S6 in the Supplementary Materials).

2.1.9. *N*-(3-(4-(((2-(6-methoxy-3-oxo-3H-xanthen-9-yl)benzoyl)oxy)methyl)-1H-1,2,3-triazol-1-yl)propyl)-*N*,*N*-dimethyltetradecan-1-aminium Bromide **11b**

It was synthesized for 30 h, with a yield of 0.194 g, 82%. ^{1}H NMR (400 MHz, DMSO-d_6, 25 °C) δ, ppm: 0.83 (t, *J* = 6.7 Hz, 3H, CH_3), 1.23 (s, 24H, 12*-CH_2-), 1.53–1.62 (m, 2H, -NCH_2-), 2.18–2.28 (m, 2H, -NCH_2-), 3.00 (s, 6H, -$N(CH_3)_2$-), 3.19–3.32 (m, 4H, -CH_2-), 3.92 (s, 3H, -OCH_3), 4.35 (t, *J* = 7.1 Hz, 2H, -NCH_2-), 5.07 (ABq, 2H, $\Delta\delta_{AB}$ = 0.09, J_{AB} = 12.5 Hz, 2H, -OCH_2-), 6.18 (d, *J* = 2.0 Hz, 1H, ArH), 6.33 (d, *J* = 9.7 Hz, 1H, ArH), 6.74 (d, *J* = 9.8 Hz, 1H, ArH), 6.79–6.91 (m, 2H, ArH), 7.18 (d, *J* = 2.4 Hz, 1H, ArH), 7.49 (d, *J* = 6.5 Hz, 1H, ArH), 7.78 (t, *J* = 6.5 Hz, 1H, ArH), 7.87 (t, *J* = 6.5 Hz, 1H, ArH), 7.91 (s, 1H, TrzH), 8.18 (d, *J* = 7.9 Hz, 1H, ArH). ^{13}C NMR (101 MHz, DMSO-d_6, 25 °C): δ, ppm: 13.9, 21.6, 22.1, 25.7, 28.5, 28.7, 28.8, 28.9, 29.0, 31.2, 46.4, 50.2, 56.3, 57.9, 60.0, 63.1, 100.5, 104.5, 113.4, 114.2, 116.7, 124.7, 128.8, 129.2, 129.5, 130.2, 130.6, 130.7, 133.3, 133.6, 140.8, 149.6, 153.6, 158.2, 163.9, 164.7, 183.8. IR (KBr) ν_{max} cm^{-1}: 3422, 2924, 2853, 1720 (C=O), 1643, 1599, 1512, 1466, 1381, 1346, 1280, 1255, 1213, 1107, 1024, 854, 758, 601. HRESI MS (*m*/*z*) $[M]^+$: calcd. for $C_{43}H_{57}N_4O_5^+$: 709.4323, found: 709.4324 (Figure S7 in the Supplementary Materials).

2.2. Photophysical and Self-Assembly Investigations

UV-visible spectra were recorded using a Shimadzu UV-2600 spectrophotometer equipped with a Shimadzu TCC-100 thermostat (Shimadzu Corporation, Kyoto, Japan).

Fluorescence spectra were performed in 10.0 mm quartz cuvettes and recorded on a Fluorolog FL-221 spectrofluorimeter (HORIBA Jobin Yvon, Kyoto, Japan) using an excitation wavelength of 430 nm with a 1 nm slit. All studies were conducted at 298 K.

DLS and ELS experiments were carried out on a Zetasizer Nano ZS instrument (Malvern Panalytical, Worcestershire, UK) with a 4 mW 633 nm He–Ne laser light source and the light-scattering angle of 173°. The data were treated with DTS software (Dispersion Technology Software 5.00). The solutions were filtered through a 0.8 μM filter before the measurements to remove dust. The experiments were carried out in the disposable plastic cells DTS 0012 (size) or in the disposable folded capillary cells DTS 1070 (zeta potential) (Malvern Panalytical, Worcestershire, UK) at 298K, with at least three experiments for each system.

2.3. General Method for Photocatalytic Reaction

A solution of photocatalyst (0.25 μmol, 0.02 eq., 0.05 mL) in acetonitrile was added to *N*-phenyl-1,2,3,4-tetrahydroisoquinoline (12.5 μmol, 1 eq.) followed by malonic ester (62.5 μmol, 5 eq.). Then, 0.2 mL of acetonitrile and 0.25 mL of bidistilled water (or 0.45 mL

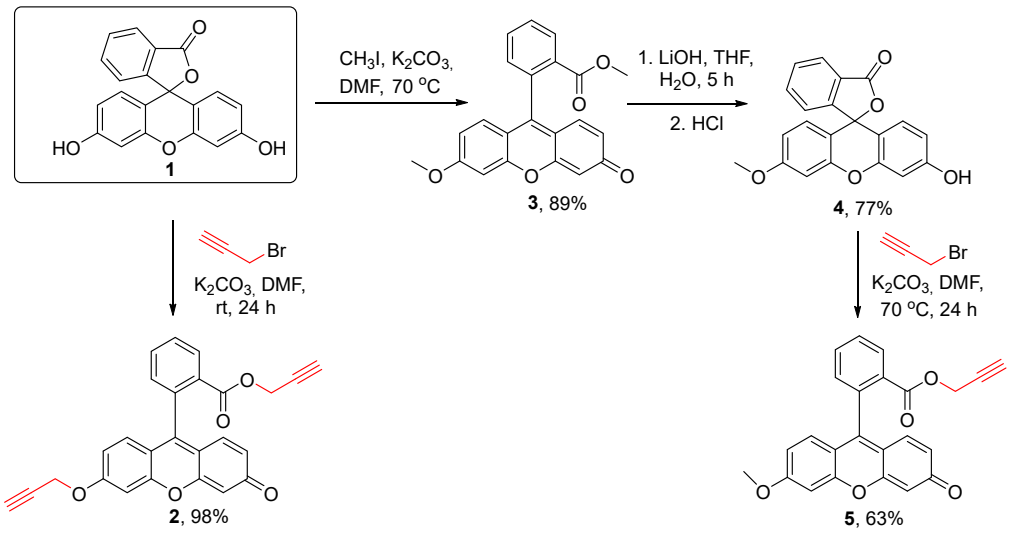
water) were also added. The exposure time by blue-light irradiation was 5 h. The progress of the reaction was monitored using gas chromatography–mass spectrometry (GC-MS). The reaction mixture was diluted to 1.5 mL with acetonitrile, so the concentration fell within the middle of the calibration curve (8.33 mmol). The final conversion was determined using ^{1}H NMR spectroscopy.

GCMS analysis was performed on a GCMS-QP2010 Ultra gas chromatograph–mass spectrometer (Shimadzu, Kyoto, Japan) equipped with an HP-5MS column (the internal diameter was 0.32 mm and the length was 30 m). The parameters were as follows: Helium 99.995% purity was the carrier gas, the temperature of an injector was 250 °C, the flow rate through the column was 2 mL/min, and the thermostat temperature program was a gradient temperature increase from 70 to 250 °C with a step of 10 °C/min. The range of scanned masses was m/z 35–400.

3. Results and Discussion

3.1. Synthesis of 1,2,3-Triazoles Containing Fragment of Fluorescein and Its Ammonium Derivatives

The copper-catalyzed cycloaddition of azides and alkynes is a versatile method for the synthesis of 1,4-disubstituted triazoles. For the synthesis of low-molecular-weight 1,2,3-triazoles containing fragments of fluorescein, several precursors for azide–alkyne cycloaddition were prepared in the first step (Scheme 1). Fluorescein **1** was reacted with an excess of propargyl bromide in the presence of K_2CO_3 to produce dipropargyl ester **2** according to a literature procedure in a 98% yield [33]. The alkylation reaction of fluorescein **1** by methyl iodide in the presence of K_2CO_3 leads to the formation of dimethyl ester **3** with an 89% yield [34]. Further hydrolysis using LiOH leads to the formation of monomethyl ester **4** in the form of a lactone form with a yield of 77% [35]. When ester **4** is introduced into the reaction with propargyl bromide, the lactone form opens under the action of the base, and the formation of ester **5** containing one triple bond occurs.



Scheme 1. Synthesis of propargyl-containing fluorescein derivatives 2 and 5.

A mono-crystal was grown for compound **5**, and the structure of the synthesized compound was confirmed by X-ray crystallography data (Figure 1). Compound **5** was also characterized using a full range of physicochemical analysis methods, including NMR ^{1}H, ^{13}C, IR, and high-resolution electrospray ionization mass spectrometry (HRESI MS).

The terminal proton of the triple bond resonates as a triplet at 2.33 ppm. As is the case with the dipropargyl derivative **2**, the methylene protons in the ester group are diastereotopic and appear as an AB quadruplet at 4.59 ppm. This characteristic specificity allows for additional monitoring of the direction of the alkylation reaction. Aromatic protons from the benzoate group appear in the weak magnetic field region as doublets at 8.27 ppm (J = 7.8 Hz) and 7.34 ppm (J = 7.2 Hz) and two triplets at 7.76 ppm and 7.68 ppm

with J = 7.4 and 7.6 Hz, respectively. The xanthene protons resonate as doublets at 6.96 ppm (J = 2.4 Hz), 6.74 ppm (J = 9.0 Hz), and 6.54 ppm (J = 9.7 Hz), and a singlet at 6.45 ppm, as well as two overlapping proton signals as a multiplet in the range 6.80–6.92 ppm. The composition of compound **5** is also defined by HRESI MS. A mono-protonated quasimolecular ion $[M+H]^+$ was found with m/z 385.1080 (calcd. for $C_{24}H_{17}O_5^+$ 385.1076). There is an absorption band in the IR spectrum corresponding to valence vibrations of the C≡CH bond at 3294 cm^{-1} (Figure S1).

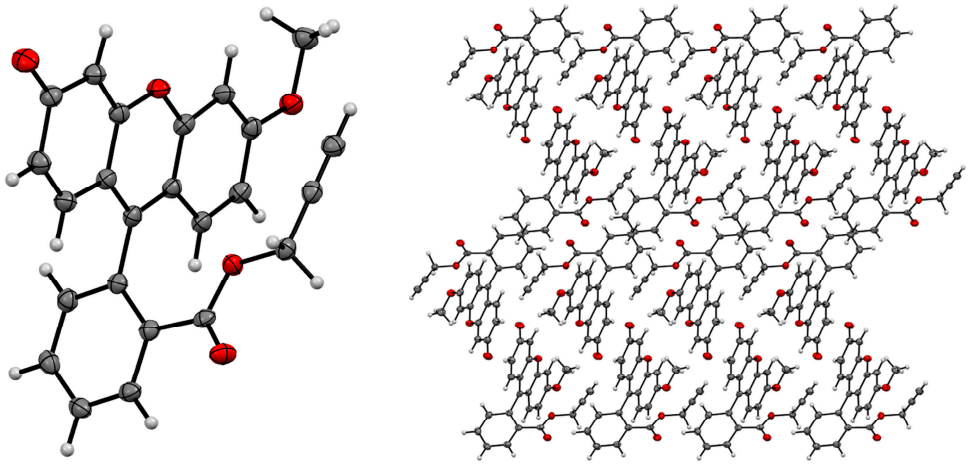
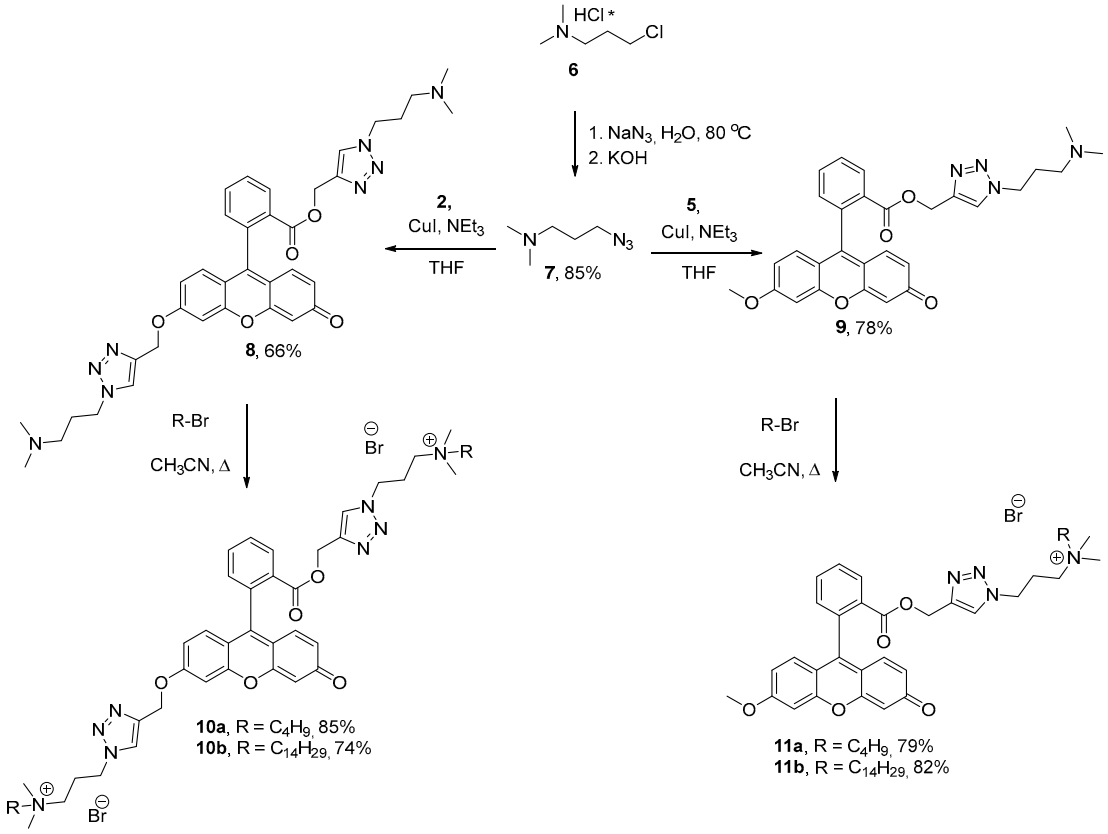


Figure 1. ORTEP representation of **5** showing 50% probability thermal ellipsoids and crystal packing of **5**. View along b axes. C atoms—grey, O atoms—red.

3-Chloro-*N*,*N*-dimethylpropan-1-amine hydrochloride **6** was used as a precursor for the synthesis of azides. Its heating in the presence of NaN_3 led to the nucleophilic substitution of chlorine with the azide functional group. After adjusting the pH of the reaction mixture to 10 with 1M KOH and extracting the product, 3-azido-*N*,*N*-dimethyl propane-1 amine **7** was obtained in a yield of 85% [36]. The presence of a tertiary amino group in the structure of azide **7** allows for further obtaining quaternized derivatives that are more soluble in water.

The next step was the CuAAC reaction of acetylenes **2** or **5** with azide **7** in the presence of the catalytic amounts of CuI in THF and triethylamine (NEt_3) as a base (Scheme 2). After the filtration through Amberlite IRA-67 and evaporation, new 1,2,3-triazoles **8** and **9** were isolated as vitreous oils with good yields. In the ^{1}H NMR spectrum of compound **8,** there is the absence of signals of terminal acetylene protons at 2.33 ppm and 2.62 ppm. Also, signals related to the *N*,*N*-dimethylaminopropyl groups are observed, with two singlets of methyl protons at 2.18 and 2.20 ppm and methylene protons at 1.98, 2.07 and 2.23–2.29 ppm). Signals of methylene protons attached to nitrogen appear as a multiplet at 4.35 ppm and a triplet at 4.46 ppm with J = 7 Hz. Methylene linkers associated with oxygen are observed as a singlet at 5.32 ppm and AB-quadruplet from diastereotopic protons at 5.11 ppm. Triazole protons appear as singlets at 7.25 and 7.72 ppm (Figure S2).

According to the HRESI MS data, there is the presence of a $[M + H]^+$ quasimolecular ion (calcd. for $C_{36}H_{41}N_8O_5^+$: 665.3200, found: 665.3200). The ^{1}H NMR spectrum of compound **9** shows proton signals of the *N*,*N*-dimethylpropyl fragment and a proton signal of the new triazole as a singlet at 7.30 ppm. The diastereotopic protons of the methylene bridge between the fluorescein fragment and the triazole appear as an AB-quadruplet at 5.14. The methylene protons of the linker between the fluoresceins and the triazoles fragments appear as a multiplet at the range of 4.29–4.38 ppm. The formation of triazole **9** is also terminated by the presence of the [M + H]+ quasimolecular ion with m/z = 513.2139, which corresponds to that calculated for $C_{29}H_{29}N_4O_5^+$ m/z = 513.2132 (Figure S3).



Scheme 2. Synthesis of mono- and diammonium derivatives of fluorescein **10a,b** and **11a,b**.

At the next step, the obtained 1,2,3-triazole derivates **8** and **9** were introduced into the quaternization reaction with one eq. of C_4H_9Br or $C_{14}H_{29}Br$ per one amino group. The competition of reaction was monitored by HRESI MS. The reaction took approximately 15–20 h for monosubstituted and 20–30 h for disubstituted fluorescein derivates. After the evaporation of the solvent and dispersion in hexane compounds **10ab** and **11ab** were obtained as viscous oil, with yields from 74% to 85%. The ammonium salts **11ab** were additionally purified using flash chromatography. On the ^{1}H NMR spectrum of dibutyl fluoresceine derivate **10a** appears signals related to the alkyl group as triplets of methyl protons at 0.87 ppm and a singlet of methylene protons at 1.88 ppm. Methylene protons, attached to quaternary nitrogen, resonate as the broad signals at 3.28 and 3.59 ppm. The composition of **10a** was well-defined by HRESI MS. The double charged $[M\text{-}2Br]^{2+}$ quasimolecular ion with m/z 389.2261 (calcd. for $C_{44}H_{58}N_8O_5^{2+}$: 389.2260) was found (Figure S4). The ^{1}H NMR spectrum of **10b** contains new signals of the alkyl substitute as a triplet at 0.86 ppm, a singlet at 1.21 ppm, and the multiplets at 3.28 and 3.59 ppm. According to the HRESI MS data, there is a presence of a quasimolecular ion $[M\text{-}2Br]^{2+}$ m/z 529.3882 (calcd. for $C_{64}H_{98}N_8O_5^{2+}$ m/z 529.3825) (Figure S5). According to the ^{1}H NMR spectra of monoquaternized fluorescein derivatives (**11ab**), the protons of the methyl moiety are evident at 0.92–0.83 ppm, and the methylene protons resonate at 1.28, 1.59 ppm for (**11a**), and 1.23 ppm for (**11b**), respectively. In the mass spectrum of compound **11a, a** quasimolecular ion $[M\text{-}Br]^+$ with m/z 569.2754 (calcd. for $C_{33}H_{37}N_4O_5^+$ m/z 569.2758) was found. And for **11b**-$[M\text{-}Br]^+$ with m/z 709.4324 (calcd. for $C_{43}H_{57}N_4O_5^+$ m/z 709.4323) was found (Figures S6 and S7).

3.2. Photophysical and Self-Assembly Properties

The next step was the study of some photophysical properties of the synthesized compounds. It was found that both fluorescein derivates (**10** with one alkyl group and **11** with two alkyl groups), exhibited fluorescent properties in the green range of the visible-

light spectrum. The change in the fluorescence intensity with respect to the concentration was studied. The spectra of all of the compounds exhibited a similar profile, with a maximum at λ_{max} = 513 nm and a shoulder at λ = 554 nm. In the case of compound **11b** with two long hydrophobic groups, the maximum was red-shifted to λ_{max} = 525 nm (Figure 2A) in regard to fluorescein. And vice versa in the absorption spectra of **10–11**, the absorption maximum shifts bathochromically in regard to fluorescein, and two maxima were observed at λ_{max} = 458 and 486 nm, with a shoulder that presents at λ = 428 nm (Figure 2B). In the case of compound **10b**, as well as in the emission spectra, a bathochromic shift at 4 nm is observed. Such a bathochromic shift indicates a change in the polarity of the surroundings and is consistent with the solvatochromic behavior of fluorescein upon transfer to nonpolar solvents [37], indirectly indicating the formation of aggregates.

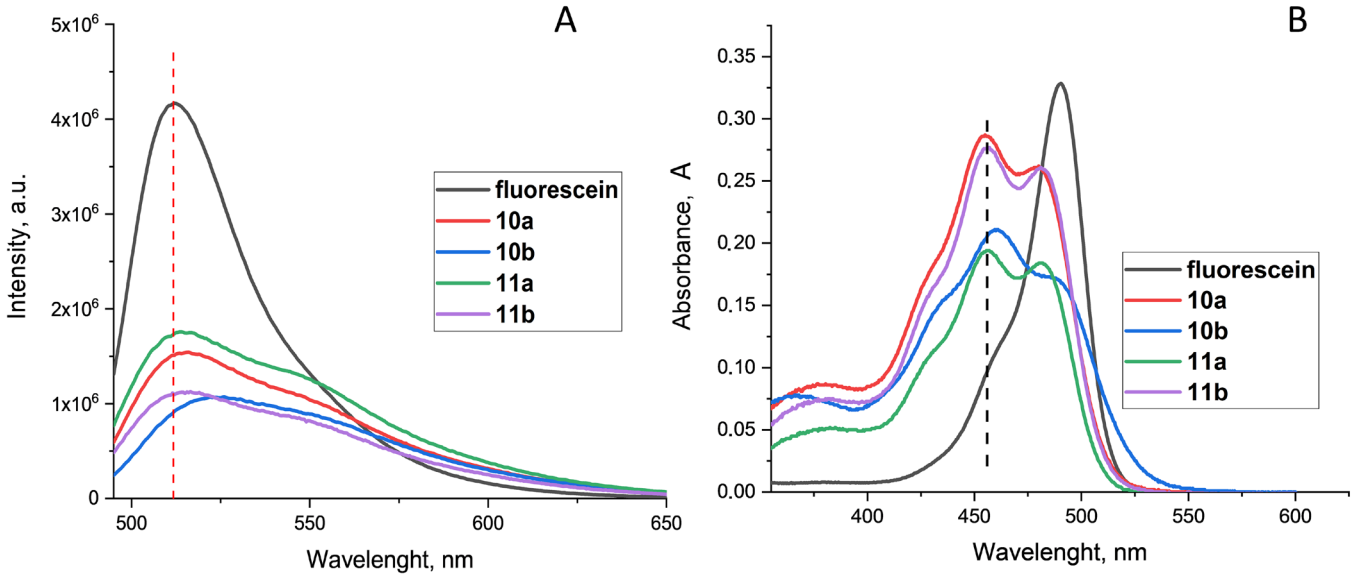


Figure 2. Emission (**A**) and absorption (**B**) spectra of fluorescein (0.1 M NaOH) and derivates **10ab** and **11ab** in water, C = 0.01 mM.

One of the most significant photophysical properties of fluorophore molecules is the fluorescent quantum yield. There are two methods for determining the quantum yield, namely absolute and relative [38]. In contrast to the absolute quantum yield, which requires the use of an integrating sphere, to determine relative yields, only emission and absorption spectra are used. So, the next step was calculating the relative quantum yield for compounds **10ab–11ab**. We used fluorescein in a 0.1 M NaOH solution for comparison purposes with the known quantum yield, which is 95% [39]. For all obtained compounds **10ab–11ab** in the concentration range of 0.01–0.05 mM, the Lambert–Bouguer–Beer law applies, and there is a linear correlation between absorption intensity and concentration. Relative quantum yield (Table 1) was calculated using emission and absorption spectra of fluorescein derivates **10ab–11ab** and Equation (1).

$$Q_s = Q_r \left(\frac{m_s}{m_r}\right)\left(\frac{n_s}{n_r}\right)^2 \quad (1)$$

where Q_s is the fluorescence quantum yield of an unknown sample, and Q_r is the fluorescence quantum yield of a known standard. m_s and m_r are the gradients of the integrated fluorescence intensity graphs depending on absorption, and n_s and n_r are the refractive indexes of the solvents used for an unknown sample and a reference, respectively [40].

Table 1. Relative quantum yield for compounds **10ab–11ab** against fluorescein disodium salt [1].

System	Q_s, % (Water with 1% DMF)
10a	16
10b	5
11a	18
11b	24

[1] Emission and absorption spectra were recorded in 10 mm quartz cell in the range of 0.01–0.1 mM.

For the fluorescein derivatives **10ab–11ab**, there was found a significant decrease in the relative quantum yield compared to the disodium salt of fluorescein. It has been shown that the highest quantum yield is observed for a monosubstituted derivative with a single tetradecyl fragment **11b**. The presence of two hydrophobic substituents leads to a decrease in quantum yield due to aggregation in the solution. The lowest quantum yield was had by compound **10a**, which is also characterized by a small bathochromic shift in the absorption and emission spectra. The correlation between fluorescence intensity and concentration of obtained derivates **10ab** and **11ab** was also studied. It is worth noting that, as the concentration increases, a significant increase in the fluorescence intensity was observed. This may be due to the formation of associates, which is accompanied by a decrease in polarity. Furthermore, further decreases in fluorescence intensity could be associated with quenching at high concentrations, where the decreased and quenched luminescence is associated with an increased number of collisions between the particles in the solution. (Figure 3). Interestingly, for all four compounds, the maximum emission intensity occurred at a C_{Imax} = 0.05 mM. The highest relative emission intensity was typically observed for the monosubstituted derivative **11b** with one tetradecyl group.

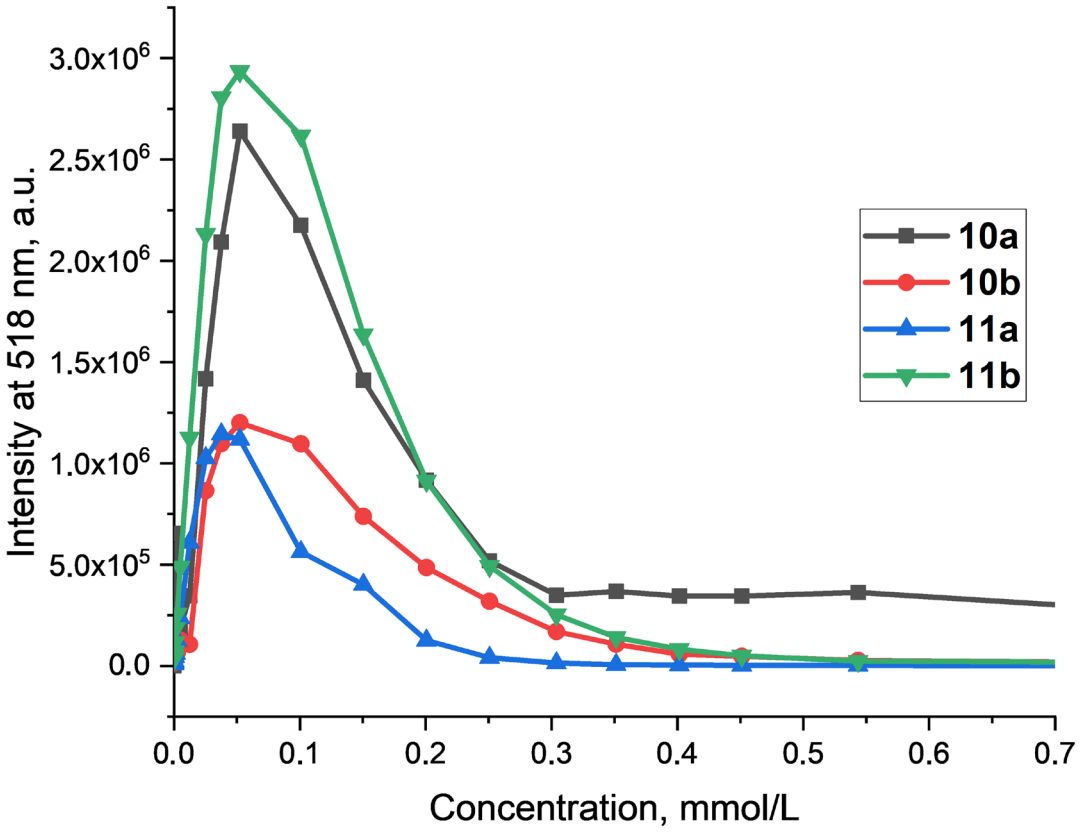


Figure 3. The dependence of the fluorescence intensity of compounds (**10ab–11ab**) on the concentration at λ = 518 nm. Concentration range: 0.08–1 mM, λ_{ex} = 430 nm, H_2O, 25 °C.

The presence of a positively charged ammonium fragment and a long hydrophobic alkyl substituent in the structure of compounds **10ab** and **11ab** creates the prerequisites for the aggregation of particles in a solution. To confirm the formation of aggregates, it was necessary to determine the critical aggregation concentration (CAC) values using the pyrene fluorescent probe [41]. CAC was determined as the value at which a change in slope was observed in the corresponding graphs of the intensity ratio between the first (373 nm) and third (383 nm) peaks in the pyrene emission spectrum (Figure 4). The polarity of pyrene decreased because of its solubilization in the hydrophobic part of the aggregates. Less-lipophilic derivatives **10a** and **11a** with one/two butyl fragments showed higher CAC values (1.43 and 0.82 mM) than the corresponding tetradecyl-containing compounds **10b** and **11b** (0.43 and 0.28 mM). Surprisingly, in contrast to classical hemini surfactants, which are characterized by a decrease in CAC compared to their single-charged analogs [42], in this case, the introduction of two lipophilic fragments leads to an increase in CAC. Such an increase can be attributed to the high rigidity of the fluorescein spacer, which prevents effective hydrophobic interactions between the alkyl moieties.

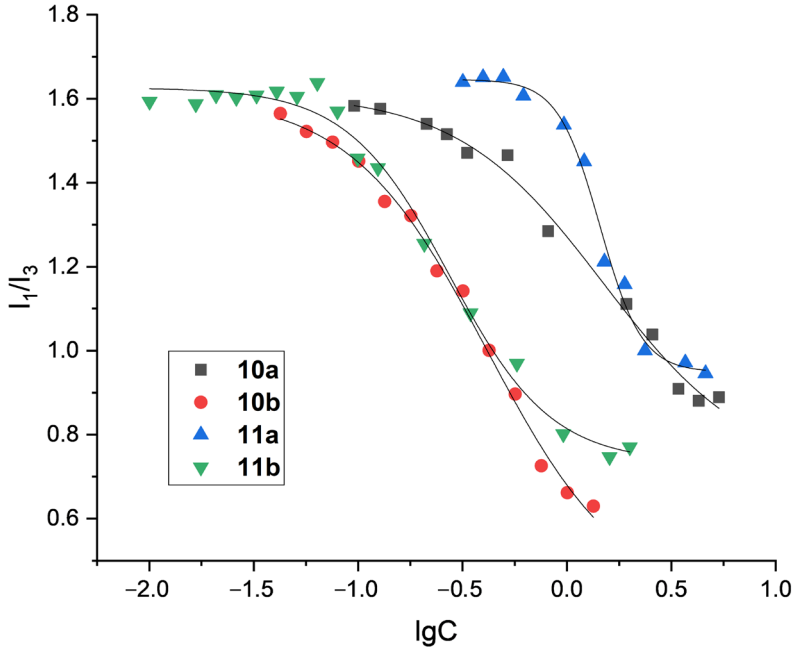


Figure 4. Dependence of the ratio of the fluorescence intensities of the first (373 nm) and third (384 nm) vibrational peaks of pyrene on the concentration of **10**–**11** in binary systems **10**/**11**—pyrene. C(pyrene) = 0.002 mM, C(fluorescein derivatives) = 0.005–5 mM.

In the next step, an experiment on dynamic light scattering to confirm the formation of aggregates was performed. At concentrations below CAC, aqueous solutions of compounds **10**–**11** formed disordered aggregates with a high polydispersity index (PDI). Above the critical concentration, all systems formed sub-micron aggregates (Table 2). The lower PDI was found for **10a**. The largest size and polydispersity index were found for **10b** with two tetradecyl substituents.

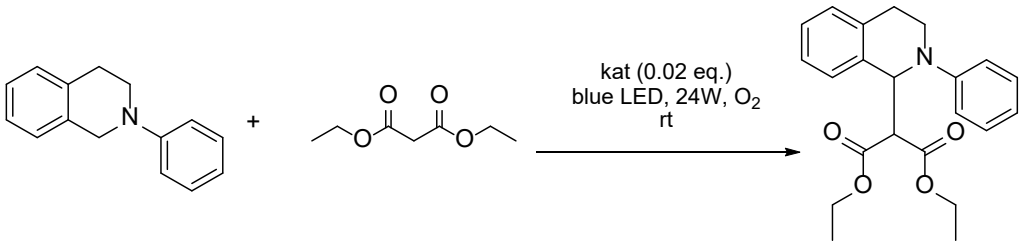
Table 2. CAC values, average hydrodynamic diameters d, and PDI of compounds **10ab**–**11ab**, H_2O, 25 °C [1].

System	10a	10b	11a	11b
CAC, mM	1.43	0.43	0.82	0.28
d, nm	165 ± 1	267 ± 25	171 ± 2	202 ± 12
PDI	0.244 ± 0.018	0.433 ± 0.029	0.429 ± 0.029	0.310 ± 0.052

[1] C (**10**, **11**) = 2 mM.

3.3. Photocatalytical Properties

Photocatalysis has become a versatile tool for C-H activation reactions of sp3-hybridized carbon atoms, allowing direct and selective C-C bond formation [43,44]. The use of photocatalysis allows for the easy generation of highly reactive iminium cations, which have been used previously in the coupling reactions of *N*-phenyl-1,2,3,4-tetrahydroisoquinoline (THI) with various carbon-containing nucleophiles [45]. Due to their unique photophysical characteristics, fluorescein and its derivatives have also become widely used as photoredox catalysts [46,47], including for reactions involving iminium ions [48]. In our study, the photocatalytic activity of amphiphilic 1,2,3-triazole derivatives of fluorescein in the model reaction of malonic ether to THI was studied (Scheme 3). The photocatalytic activity of fluorescein derivatives was carried out in pure acetonitrile and acetonitrile–water mixtures. The reaction mixture was irradiated for 5 h at room temperature using a 24 w blue-LED photoreactor (Figure S8).



Scheme 3. Model reaction of condensation of TGI with malonic ester.

The conversion of the initial THI was evaluated by gas chromatography–mass spectrometry (GC-MS), using an absolute calibration method (Figure S9, Table 3). The method of reaction estimation by the product calibration line was not used because two peaks were recorded in the GC-MS spectra, namely the product peak (m/z = 367) and the peak corresponding to the product decomposition (m/z = 208). The ratio of these peaks varied, which can be explained by the fact that the product decomposed during evaporation in the injector. In addition to GC-MS, the product yield was estimated from the integrated intensity of the TGI (product) CH proton signal at 5.57 ppm relative to the TGI (reagent) CH_2 proton signal at 4.27 ppm (Figure S10).

Table 3. THI conversion (GCMS) or product yield (^{1}H-NMR) in the reaction of THI with malonic ester in the presence of 0.02 equiv. of **10ab**, **11ab** [1].

Entry	Catalyst	GCMS Conversion, %	^{1}H-NMR Yield, %
1	10a *	87	94
2	10a **	87	95
3	10a ***	92	94
4	10b *	86	93
5	10b **	86	94
6	10b ***	84	90
7	11a *	86	91
8	11a **	87	91
9	11a ***	66	71
10	11b *	84	87
11	11b **	87	89
12	11b ***	95	100
13	11b ****	1	0
14	No catalyst	0	0
15	1 (disodium salt) ***	81	84

[1] A 12.5 µmol THI, 0.25 µmol of catalyst, 62.5 µmol malonic ester, blue LED. * Reaction in CH_3CN. ** Reaction in CH_3CN-water 50:50. *** Reaction in CH_3CN-water 10:90. **** Reaction in CH_3CN-water 10:90 without light.

In all cases, the product yield by ^{1}H NMR was higher than the conversion by GC-MS on average by 5%, which is due to the lower sensitivity of the NMR method. When the reaction was carried out in pure acetonitrile, the GC-MS conversion did not reach 90% (entries 1, 4, 7, and 10). Similar data were obtained at 50% water content (entries 2, 5, 8, and 11). At the transition to 90% water content (entries 3, 6, 9, 12), the photocatalysts began to behave differently. The lowest conversion was demonstrated by **11a**, and its analog **11b,** having a tetradecyl fragment, on the contrary, was the best, demonstrating 95% conversion by GC-MS and 100% product formation on ^{1}H NMR. Notably, when catalyst **11b** was used without light, the reaction did not proceed (entry 13), nor did the reaction proceed without the catalyst (entry 14). With the initial fluorescein disodium salt (entry 15), the conversion was 81%, thus showing the better efficiency of system **11b**. The data obtained are consistent with the fact that **11b** has the highest quantum yield in the series. Also, **11b** has the lowest CAC value in the series. A positive contribution of micellar catalysis [49] in this case is highly probable.

4. Conclusions

- New 1,2,3-triazole derivatives of fluorescein containing one or two fragments of tertiary amines and their ammonium salts were synthesized for the first time. The structures of these compounds were confirmed by a wide range of physical and chemical methods;
- Values of the critical aggregation concentrations were obtained for ammonium salts. The formation of aggregates was also confirmed by dynamic light-scattering experiments. It has been shown that the presence of one or two hydrophobic tetradecyl fragments in the structure of a fluorescein derivative leads to an increase in the size of the aggregates. The smallest size of the aggregates and the polydispersity index were recorded for a derivative with two butyl substituents in the structure;
- The study of photocatalytic activity using the model-coupling reaction of malonic ester with *N*-phenyl 1,2,3,4-tetrahydroisoquinoline under the blue LED light showed good efficiency for all derivatives. However, the conversion of the initial THI reached 100% when compound **11b**, containing a tetradecyl substituent, was used. These data confirmed the calculation of the quantum yield, which gave the best value for compound **11b**.

Supplementary Materials: The following supporting information can be downloaded at https://www.mdpi.com/article/10.3390/org5030018/s1: Figure S1: NMR ^{1}H (a), ^{13}C (b), FT IR (c) and HRESI MS (d) spectra of prop-2-yn-1-yl 2-(6-methoxy-3-oxo-3H-xanthen-9-yl)benzoate (**5**); Figure S2: NMR ^{1}H (a), ^{13}C (b), FT IR (c) and HRESI MS (d) spectra of (1-(3-(dimethylamino)propyl)-1H-1,2,3-triazol-4-yl)methyl 2-(6-((1-(3-(dimethylamino)propyl)-1H-1,2,3-triazol-4-yl)methoxy)-3-oxo-3H-xanthen-9-yl)benzoate (**8**); Figure S3: NMR ^{1}H (a), ^{13}C (b), FT IR (c) and HRESI MS (d) spectra of (1-(3-(dimethylamino)propyl)-1H-1,2,3-triazol-4-yl)methyl 2-(6-methoxy-3-oxo-3H-xanthen-9-yl)benzoate (**9**); Figure S4: NMR ^{1}H (a), ^{13}C (b), FT IR (c) and HRESI MS (d) spectra of *N*-(3-(4-(((2-(6-((1-(3-(butyldimethylammonio)propyl)-1H-1,2,3-triazol-4-yl)methoxy)-3-oxo-3H-xanthen-9-yl)benzoyl)oxy)methyl)-1H-1,2,3-triazol-1-yl)propyl)-*N*,*N*-dimethylbutan-1-aminium bromide (**10a**); Figure S5: NMR ^{1}H (a), ^{13}C (b), FT IR (c) and HRESI MS (d) spectra of *N*-(3-(4-(((2-(6-((1-(3-(dimethyl(tetradecyl)ammonio)propyl)-1H-1,2,3-triazol-4-yl)methoxy)-3-oxo-3H-xanthen-9-yl)benzoyl)oxy)methyl)-1H-1,2,3-triazol-1-yl)propyl)-*N*,*N*-dimethyltetradecan-1-aminium bromide (**10b**); Figure S6: NMR ^{1}H (a), ^{13}C (b), FT IR (c) and HRESI MS (d) spectra of *N*-(3-(4-(((2-(6-methoxy-3-oxo-3H-xanthen-9-yl)benzoyl)oxy)methyl)-1H-1,2,3-triazol-1-yl)propyl)-*N*,*N*-dimethylbutan-1-aminium bromide (**11a**); Figure S7: NMR ^{1}H (a), ^{13}C (b), FT IR (c) and HRESI MS (d) spectra of *N*-(3-(4-(((2-(6-methoxy-3-oxo-3H-xanthen-9-yl)benzoyl)oxy)methyl)-1H-1,2,3-triazol-1-yl)propyl)-*N*,*N*-dimethyltetradecan-1-aminium bromide (**11b**); Figure S8: Photo of a 24W LED air-cooled photoreactor; Figure S9: Plot of the GC-MS peak area of N-phenyl-1,2,3,4-tetrahydroisoquinoline vs. its concentration; Figure S10: ^{1}H NMR spectrum of the reaction of THI with malonic ester in the presence of **11b** ($CDCl_3$).

Author Contributions: Conceptualization, V.B., I.A., S.S. and E.S.; methodology, V.B. and E.S.; investigation, A.A. (Alina Artemenko), A.A. (Aliya Akhatova), E.B., D.I., K.U. and D.M.; resources, I.A.; data curation, V.B., D.I. and E.B.; writing—original draft preparation, A.A. (Alina Artemenko) and A.A. (Aliya Akhatova); writing—review and editing, V.B.; visualization, V.B.; supervision, V.B.; project administration, V.B.; funding acquisition, V.B. All authors have read and agreed to the published version of the manuscript.

Funding: This research was funded by the Russian Science Foundation, grant number 21-73-10062.

Data Availability Statement: Data are contained within the article or Supplementary Materials.

Conflicts of Interest: The authors declare no conflicts of interest.

References

1. Ardila-Fierro, K.J.; Hernández, J.G. Sustainability Assessment of Mechanochemistry by Using the Twelve Principles of Green Chemistry. *ChemSusChem* **2021**, *14*, 2145–2162. [CrossRef] [PubMed]
2. Ganesh, K.N.; Zhang, D.; Miller, S.J.; Rossen, K.; Chirik, P.J.; Kozlowski, M.C.; Zimmerman, J.B.; Brooks, B.W.; Savage, P.E.; Allen, D.T.; et al. Green Chemistry: A Framework for a Sustainable Future. *Org. Process Res. Dev.* **2021**, *25*, 1455–1459. [CrossRef]
3. Bobo, M.V.; Kuchta, J.J.; Vannucci, A.K. Recent Advancements in the Development of Molecular Organic Photocatalysts. *Org. Biomol. Chem.* **2021**, *19*, 4816–4834. [CrossRef] [PubMed]
4. Lanjwani, M.F.; Tuzen, M.; Khuhawar, M.Y.; Saleh, T.A. Trends in Photocatalytic Degradation of Organic Dye Pollutants Using Nanoparticles: A Review. *Inorg. Chem. Commun.* **2024**, *159*, 111613. [CrossRef]
5. Ramar, S.; Elango, P.; Velusamy, A.; Athinarayanan, B.; Jothi, V.K.; Hsu-Wei; Pattappan, D.; Gurusamy, A.; Lai, Y.-T. An Eco-Safety g-C_3N_4/Nb_2O_5/Ag Ternary Nanocomposite for Photocatalytic Degradation of Pharmaceutical Wastes and Dyes in Wastewater and Zebrafish Embryonic Assessment. *J. Mol. Struct.* **2024**, *1317*, 139127. [CrossRef]
6. Ramasundaram, S.; Balasankar, A.; Arokiyaraj, S.; Sumathi, P.; Hwan Oh, T. Multi-Usable Titanium Dioxide and Poly(Vinylidene Fluoride) Composite Foam Photocatalyst for Degradation of Organic Pollutants. *Appl. Surf. Sci.* **2023**, *609*, 155264. [CrossRef]
7. Li, D.; Shi, W. Recent Developments in Visible-Light Photocatalytic Degradation of Antibiotics. *Cuihua Xuebao/Chin. J. Catal.* **2016**, *37*, 792–799. [CrossRef]
8. Koe, W.S.; Lee, J.W.; Chong, W.C.; Pang, Y.L.; Sim, L.C. An Overview of Photocatalytic Degradation: Photocatalysts, Mechanisms, and Development of Photocatalytic Membrane. *Environ. Sci. Pollut. Res.* **2020**, *27*, 2522–2565. [CrossRef]
9. Kumari, H.; Sonia; Suman; Ranga, R.; Chahal, S.; Devi, S.; Sharma, S.; Kumar, S.; Kumar, P.; Kumar, S.; et al. *A Review on Photocatalysis Used for Wastewater Treatment: Dye Degradation*; Springer International Publishing: New York, NY, USA, 2023; Volume 234, ISBN 0123456789.
10. Hari, D.P.; Hering, T.; König, B. Visible Light Photocatalytic Synthesis of Benzothiophenes. *Org. Lett.* **2012**, *14*, 5334–5337. [CrossRef]
11. Song, L.; Wang, W.; Yue, J.-P.; Jiang, Y.-X.; Wei, M.-K.; Zhang, H.-P.; Yan, S.-S.; Liao, L.-L.; Yu, D. Visible-Light Photocatalytic Di- and Hydro-Carboxylation of Unactivated Alkenes with CO_2. *Nat. Catal.* **2022**, *5*, 832–838. [CrossRef]
12. Dissanayake, K.C.; Ebukuyo, P.O.; Dhahir, Y.J.; Wheeler, K.; He, H. A BODIPY-Functionalized PdII Photoredox Catalyst for Sonogashira C-C Cross-Coupling Reactions. *Chem. Commun.* **2019**, *55*, 4973–4976. [CrossRef] [PubMed]
13. Zhou, Z.; Yang, J.; Yang, B.; Han, Y.; Zhu, L.; Xue, X.S.; Zhu, F. Photoredox Nickel-Catalysed Stille Cross-Coupling Reactions. *Angew. Chem. Int. Ed.* **2023**, *62*, e202314832. [CrossRef] [PubMed]
14. Zhou, C.; Lei, T.; Wei, X.Z.; Ye, C.; Liu, Z.; Chen, B.; Tung, C.H.; Wu, L.Z. Metal-Free, Redox-Neutral, Site-Selective Access to Heteroarylamine via Direct Radical−radical Cross-Coupling Powered by Visible Light Photocatalysis. *J. Am. Chem. Soc.* **2020**, *142*, 16805–16813. [CrossRef] [PubMed]
15. Jati, A.; Dey, K.; Nurhuda, M.; Addicoat, M.A.; Banerjee, R.; Maji, B. Dual Metalation in a Two-Dimensional Covalent Organic Framework for Photocatalytic C-N Cross-Coupling Reactions. *J. Am. Chem. Soc.* **2022**, *144*, 7822–7833. [CrossRef] [PubMed]
16. Zavalishin, M.N.; Gamov, G.A.; Kiselev, A.N.; Nikitin, G.A. A Fluorescein Conjugate as Colorimetric and Red-Emissive Fluorescence Chemosensor for Selective Recognition Cu^{2+} Ions. *Opt. Mater.* **2024**, *153*, 115580. [CrossRef]
17. Wagay, S.A.; Alam, M.; Ali, R. Synthesis of Two Novel Fluorescein Appended Dipyromethanes (DPMs): Naked-Eye Chemosensors for Fluoride, Acetate and Phosphate Anions. *J. Mol. Struct.* **2023**, *1291*, 135982. [CrossRef]
18. Keerthana, S.; Sam, B.; George, L.; Sudhakar, Y.N.; Varghese, A. Fluorescein Based Fluorescence Sensors for the Selective Sensing of Various Analytes. *J. Fluoresc.* **2021**, *31*, 1251–1276. [CrossRef]
19. Li, Z.; Song, H.; Guo, R.; Zuo, M.; Hou, C.; Sun, S.; He, X.; Sun, Z.; Chu, W. Visible-Light-Induced Condensation Cyclization to Synthesize Benzimidazoles Using Fluorescein as a Photocatalyst. *Green Chem.* **2019**, *21*, 3602–3605. [CrossRef]
20. Tu, X.P.; Wei, L.L.; Zhang, K.X.; Chen, Y.; Zhou, M.D. Synthesis of Fluorescein-Containing Polymeric Heterogeneous Photocatalyst and Its Applications. *Tetrahedron* **2024**, *160*, 134028. [CrossRef]
21. Sun, W.; Chen, H.; Wang, K.; Wang, X.; Lei, M.; Liu, C.; Zhong, Q. Synthesis of Benzothiazoles Using Fluorescein as an Efficient Photocatalyst under Visible Light. *Mol. Catal.* **2021**, *510*, 111693. [CrossRef]

22. Wang, Y.; Li, J.; Zhou, Z.; Zhou, R.; Sun, Q.; Wu, P. Halo-Fluorescein for Photodynamic Bacteria Inactivation in Extremely Acidic Conditions. *Nat. Commun.* **2021**, *12*, 526. [CrossRef] [PubMed]
23. Pinto, A.; Llanos, A.; Gomila, R.M.; Frontera, A.; Rodríguez, L. Ligand and Gold(I) Fluorescein-AIEgens as Photosensitizers in Solution and Doped Polymers. *Inorg. Chem.* **2023**, *62*, 7131–7140. [CrossRef] [PubMed]
24. Gaigalas, A. Measurement of the Fluorescence Quantum Yield Using a Spectrometer With an Integrating Sphere Detector. *J. Res. Natl. Inst. Stand. Technol.* **2008**, *113*, 17–28. [CrossRef] [PubMed]
25. Rajasekar, M. Recent Development in Fluorescein Derivatives. *J. Mol. Struct.* **2021**, *1224*, 129085. [CrossRef]
26. Russo, C.; Brunelli, F.; Tron, G.C.; Giustiniano, M. Visible-Light Photoredox Catalysis in Water. *J. Org. Chem.* **2023**, *88*, 6284–6293. [CrossRef]
27. Cortes-Clerget, M.; Yu, J.; Kincaid, J.R.A.; Walde, P.; Gallou, F.; Lipshutz, B.H. Water as the Reaction Medium in Organic Chemistry: From Our Worst Enemy to Our Best Friend. *Chem. Sci.* **2021**, *12*, 4237–4266. [CrossRef]
28. Pallini, F.; Sangalli, E.; Sassi, M.; Roth, P.M.C.; Mattiello, S.; Beverina, L. Selective Photoredox Direct Arylations of Aryl Bromides in Water in a Microfluidic Reactor. *Org. Biomol. Chem.* **2021**, *19*, 3016–3023. [CrossRef]
29. Artemenko, A.A.; Burilov, V.A.; Solov'eva, S.E.; Antipin, I.S. Covalent and Supramolecular Conjugates of Calixarenes with Some Fluorescent Dyes of the Xanthene Series. *Colloid J.* **2022**, *84*, 563–580. [CrossRef]
30. Sheldrick, G.M. SHELXT—Integrated Space-Group and Crystal-Structure Determination. *Acta Crystallogr. Sect. A Found. Adv.* **2015**, *71*, 3–8. [CrossRef]
31. Sheldrick, G. A Short History of ShelX. *Acta Crystallogr. A* **2008**, *64*, 112–122. [CrossRef]
32. Macrae, C.; Edgington, P.; McCabe, P.; Pidcock, E.; Shields, G.; Taylor, R.; Towler, M.; van de Streek, J. Mercury: Visualization and Analysis of Crystal Structures. *J. Appl. Crystallogr.* **2006**, *39*, 453–457. [CrossRef]
33. Berscheid, R.; Nieger, M.; Vögtle, F. Konkave Farbstoffmoleküle Vom Triphenylmethan-Typ. *Chem. Ber.* **1992**, *125*, 2539–2552. [CrossRef]
34. Xiang, Y.; He, B.; Li, X.; Zhu, Q. The Design and Synthesis of Novel "Turn-on" Fluorescent Probes to Visualize Monoamine Oxidase-B in Living Cells. *RSC Adv.* **2013**, *3*, 4876–4879. [CrossRef]
35. Du, L.; Risinger, A.L.; Yee, S.S.; Ola, A.R.B.; Zammiello, C.L.; Cichewicz, R.H.; Mooberry, S.L. Identification of C-6 as a New Site for Linker Conjugation to the Taccalonolide Microtubule Stabilizers. *J. Nat. Prod.* **2019**, *82*, 583–588. [CrossRef] [PubMed]
36. Carboni, B.; Benalil, A.; Vaultier, M. Aliphatic Amino Azides as Key Building Blocks for Efficient Polyamine Syntheses. *J. Org. Chem.* **1993**, *58*, 3736–3741. [CrossRef]
37. Cheptea, C.; Zara, A.; Ambrosi, E.; Morosanu, A.C.; Diaconu, M.; Miron, M.; Dorohoi, D.O.; Dimitriu, D.G. On the Solvatochromism of Fluorescein Sodium. *Symmetry* **2024**, *16*, 673. [CrossRef]
38. Lakowicz, J.R. *Principles of Fluorescence Spectroscopy, 3rd Principles of Fluorescence Spectroscopy*, 3rd ed.; Springer: New York, NY, USA, 2006; ISBN 0387312781.
39. Shen, J.; Snook, R.D. Thermal Lens Measurement of Absolute Quantum Yields Using Quenched Fluorescent Samples as References. *Chem. Phys. Lett.* **1989**, *155*, 583–586. [CrossRef]
40. Kandi, D.; Mansingh, S.; Behera, A.; Parida, K. Calculation of Relative Fluorescence Quantum Yield and Urbach Energy of Colloidal CdS QDs in Various Easily Accessible Solvents. *J. Lumin.* **2021**, *231*, 117792. [CrossRef]
41. Piñeiro, L.; Novo, M.; Al-Soufi, W. Fluorescence Emission of Pyrene in Surfactant Solutions. *Adv. Colloid Interface Sci.* **2015**, *215*, 1–12. [CrossRef]
42. Vasileva, L.; Gaynanova, G.; Valeeva, F.; Romanova, E.; Pavlov, R.; Kuznetsov, D.; Belyaev, G.; Zueva, I.; Lyubina, A.; Voloshina, A.; et al. Synthesis, Properties, and Biomedical Application of Dicationic Gemini Surfactants with Dodecane Spacer and Carbamate Fragments. *Int. J. Mol. Sci.* **2023**, *24*, 12312. [CrossRef]
43. Dumur, F.; Lalevée, J. Recent Advances in Photoredox Catalysts. *Catalysts* **2024**, *14*, 26. [CrossRef]
44. Romero, N.A.; Nicewicz, D.A. Organic Photoredox Catalysis. *Chem. Rev.* **2016**, *116*, 10075–10166. [CrossRef] [PubMed]
45. Franz, J.F.; Kraus, W.B.; Zeitler, K. No Photocatalyst Required-Versatile, Visible Light Mediated Transformations with Polyhalomethanes. *Chem. Commun.* **2015**, *51*, 8280–8283. [CrossRef] [PubMed]
46. Choi, W.O.; Jung, Y.J.; Kim, M.; Kim, H.; Li, J.; Ko, H.; Lee, H.I.; Lee, H.J.; Lee, J.K. Substituent Effects of Fluorescein on Photoredox Initiating Performance under Visible Light. *ACS Omega* **2023**, *8*, 40277–40286. [CrossRef]
47. Singh, P.; Yadav, R.K.; Kim, T.W.; Kumar, A.; Dwivedi, D.K. Chitosan-Based Fluorescein Isothiocyanate Film as a Highly Efficient Metal-Free Photocatalyst for Solar-Light-Mediated Direct C-H Arylation. *Int. J. Energy Res.* **2021**, *45*, 5964–5973. [CrossRef]
48. Hari, D.P.; König, B. Eosin Y Catalyzed Visible Light Oxidative C–C and C–P Bond Formation. *Org. Lett.* **2011**, *13*, 3852–3855. [CrossRef]
49. Acharjee, A.; Rakshit, A.; Chowdhury, S.; Saha, B. Micelle Catalysed Conversion of 'on Water' Reactions into 'in Water' One. *J. Mol. Liq.* **2021**, *321*, 114897. [CrossRef]

Disclaimer/Publisher's Note: The statements, opinions and data contained in all publications are solely those of the individual author(s) and contributor(s) and not of MDPI and/or the editor(s). MDPI and/or the editor(s) disclaim responsibility for any injury to people or property resulting from any ideas, methods, instructions or products referred to in the content.